PERGAMON

Journal of Structural Geology 23 (2001) 531–543

JOURNAL OF STRUCTURAL GEOLOGY

www.elsevier.nl/locate/jstrugeo

A palaeoseismological and geoarchaeological investigation of the Eliki fault, Gulf of Corinth, Greece

Ioannis K. Koukouvelas[a,*], Leonidas Stamatopoulos[a], Dora Katsonopoulou[b], Spyros Pavlides[c]

[a]*Department of Geology, Division of Physical Marine Geology and Geodynamics, University of Patras, 265 00 Patras, Greece*
[b]*The Helike Society, Poste Restante 25 003 Diakopto, Achaia, Greece*
[c]*Department of Geology and Physical Geography, Aristotle University of Thessaloniki, GR-54006 Thessaloniki, Greece*

Received 24 January 2000; accepted 31 July 2000

Abstract

Palaeoseismological and morphotectonic analyses enable us to define a 400-m-wide actively deformed zone associated with the active Eliki normal fault, central Greece, bounded on the south by a second-order fault and on the north by a composite and prominent fault scarp. This scarp is further analysed by trenching. Based on colluvium stratigraphy, displacement of distinct horizons and deposition of sedimentary layers, three faulting events have been identified along four fault strands affecting unconsolidated sediments in the trench. The two younger events, with throws of 0.93 and 1.37 m, respectively, the third event, with a throw of 0.44 m, and the penultimate 373 BC event suggest a variable seismic history.

The entire alluvial plain of the Kerynitis and Vouraikos rivers, which cross the Eliki fault, has subsided at a rate of 1.4 mm/year, resulting in the burial of the Late Hellenistic–Roman occupation horizons under 3 m of fluvial and colluvial sediments in places.

Extension in the broader area is accommodated by the seismically active Eliki and Egion faults. Structural and palaeoseismological analysis of those two faults indicates that they accommodate 1.5 mm/year, or about 10% of the geodetically estimated extension of up to 13 mm/year.

1. Introduction

Evidence of active tectonism in the Aegean region is found in active faults bounding sedimentary basins and the occurrence of earthquakes, as noted from archaeological excavations and mentioned in historical records (Doutsos and Piper, 1990; Guidoboni, 1994; Stiros and Jones, 1996; Papazachos and Papazachou, 1997; Nur and Cline, 2000) and from present day seismicity (Fig. 1a). Although the geotectonic context of this seismicity is well understood, the coupling between plate motions and seismicity is poorly known due to the complex interaction of a series of lithospheric plates (Fig. 1b) (Jackson and McKenzie, 1988; Billiris et al., 1991; Jackson, 1994; Papazachos et al., 1999). Nevertheless, despite the general complexity of plate interaction, the present day seismicity in the Aegean area is concentrated along specific structural zones, such as in the North Aegean Trough (see Pavlides et al., 1990, and citations therein) and the Gulf of Corinth (Koukouvelas et al., 1996; Jackson, 1999) (Fig. 1a).

In the Gulf of Corinth, the seismicity occurs on 10- to 40-km-long normal faults, such as the Eliki fault, which is one of the most prominent of these faults in the gulf (Fig. 1c). Observations that support long-term active deformation in the Gulf include the rapid uplift of its southern flank, the reversal of drainages, short northward-flowing rivers deeply incised into their former fluvial and deltaic deposits, and the presence of strips of fresh limestone at the base of prominent fault scarps (Doutsos and Piper, 1990; Collier et al., 1992; Koukouvelas, 1998b; Koukouvelas et al., 1999). Fault rupturing events over this area are limited or not described, and we know of only three earthquakes that produced surface rupture. Two of these located in the study area are the 1861 Eliki earthquake and the 1995 Egion earthquake (Schmidt, 1879; Koukouvelas and Doutsos, 1996). The third is the 1981 Corinthian earthquake sequence located near the eastern end of the Gulf of Corinth (Jackson et al., 1982) (Fig. 1c).

Palaeoseismological studies through trenching investigations of fault colluvial tectonostratigraphy can extend historical seismicity data and are therefore a valuable method that can provide data regarding the occurrence of destructive prehistoric earthquakes (Crone and Omdahl, 1987; McCalpin, 1996; Pavlides et al., 1999). These data are important for hazard assessment in areas with relatively

* Corresponding author. Tel. and fax: +30-61-994-485.
E-mail address: iannis@patreas.upatras.gr (I.K. Koukouvelas).

0191-8141/01/$ - see front matter
PII: S0191-8141(00)00124-3

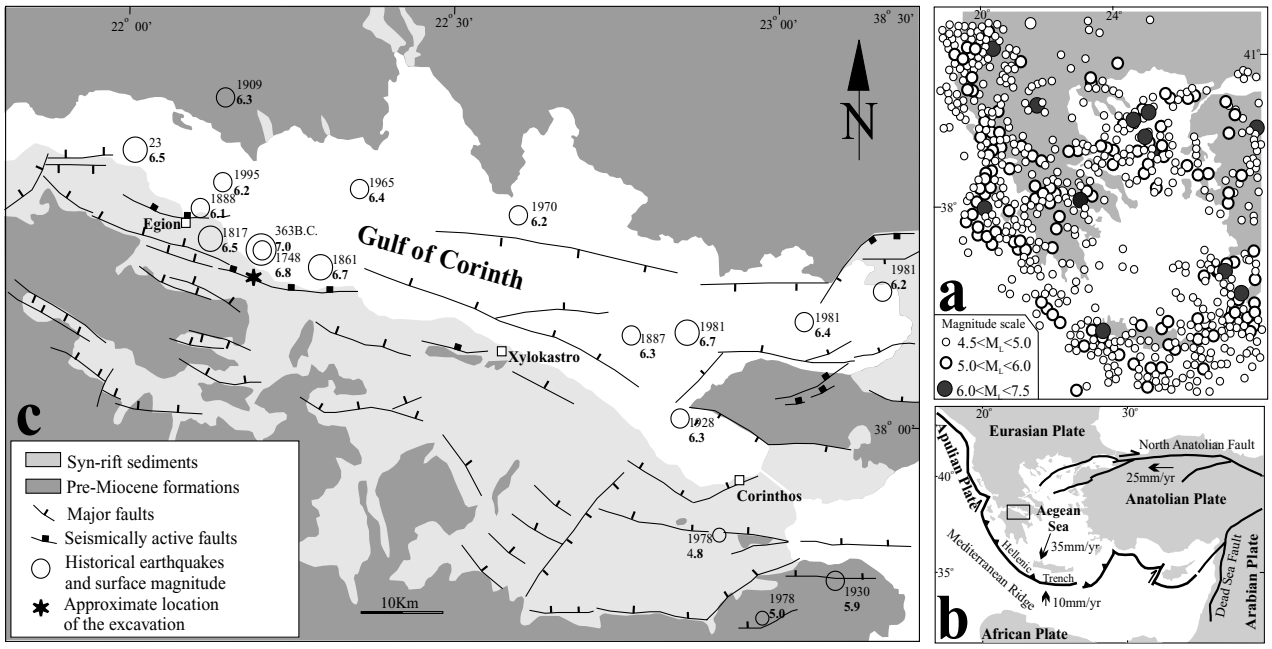

Fig. 1. (a) Seismicity map of Greece for the period from 1964 to 1998 (data from National Observatory of Athens, 1999). (b) Map showing major geotectonic elements and interacting plates in the Aegean area, rectangle shows the location of part c (modified from Jackson and McKenzie, 1988; Papazachos and Papazachou, 1997; Nur and Cline, 2000). Motion vectors of the North Anatolian fault after Le Pichon et al. (1995), and of the Aegean and African plates relative to Eurasia after Kahle et al. (1998). (c) Map showing major faults of the Gulf of Corinth and historical seismicity; star shows the study area in approximation. Fault pattern from Koukouvelas and Doutsos (1996), Collier et al. (1998), and Koukouvelas et al. (1999). Historical seismicity after Ambraseys and Jackson (1990), Papazachos and Papazachou (1997).

low instrumentally recorded seismic activity (Pavlides, 1996; Chatzipetros et al., 1998) or in the testing of rupture models in areas of high seismicity, like the Gulf of Corinth (Roberts and Koukouvelas, 1996). However, previous palaeoseismological excavations along active faults in the Gulf of Corinth have focused only towards the eastern part of the gulf (Collier et al., 1998) (Fig. 1c). The study presented here is the first along the Eliki fault in the western part of the Gulf of Corinth.

Palaeoseismological observations in the Eliki area are also important for understanding the relationship between active tectonism and the location of ancient Helike. This famous city, which was the capital of the Achaean Dodekapolis, was located southeast of present day Egion and was destroyed during the winter of 373 BC by a strong earthquake (Soter and Katsonopoulou, 1999, and citations therein). Finally, palaeoseismological data can help us to analyse the deficit between the strain estimated by the earthquake events and GPS measurements. Indeed, GPS measurements in the interval 1989–1997 (Clarke et al., 1998), as well as an analysis of the geology (Doutsos et al., 1988), suggest that the rate of extension across the Gulf of Corinth increases from east to west.

In this study, we assess the most important fault of the western part of the Gulf of Corinth in terms of historical seismicity, its morphotectonic expression and its palaeoseismicity. The re-evaluation of the historical seismicity, as well as the identification and mapping of a series of fault scarps, allowed us to define most of the deformed zone across the fault and an assessment of the segmentation along the fault. The morphotectonic imprint of the fault is analysed with the measurement of the incision/widening ratio of streams draining the fault scarp. Detailed analysis of the colluvial tectonostratigraphy exposed in trenches, along with dating of pottery fragments and bones found in the most important of the three excavations, enabled us to resolve the palaeoseismological activity of the Eliki fault. Finally, we discuss the implication of palaeoseismological fault displacements on the palaeogeography, archaeology and the long-term rate of deformation of the study area.

2. Geological setting

Five active normal faults to the south of the Egion area (Fig. 2, inset) control the accumulation of sediments at the western end of the Gulf of Corinth. Active deformation in that area is shown by historical earthquakes and reports of active slip during the 1861 and 1995 events, the bending of rivers (Fig. 2), the presence of prominent fault scarps, the occurrence of hill front landslides, the uplift of river terraces and shorelines, the fault-related incisions of valleys, the rapid uplift of modern fan deltas, and the occurrence of submarine landslides (Koukouvelas and Doutsos, 1996; Stewart, 1996; Soter, 1998; Koukouvelas, 1998b).

The Eliki and Egion normal faults are the northernmost two faults that affect the south coast of the Gulf of Corinth in the study area (Fig. 2). The 40-km-long Eliki fault, which in

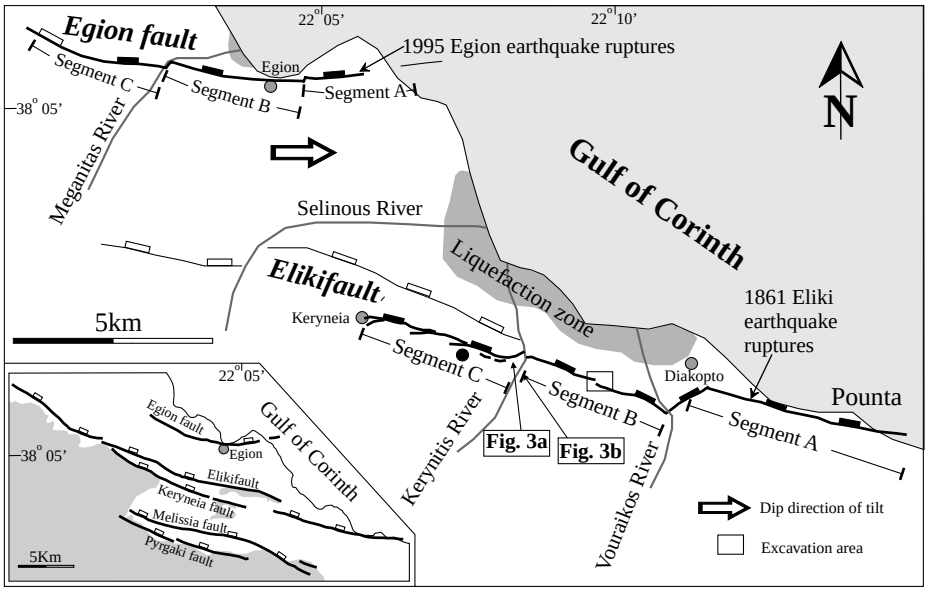

Fig. 2. Tectonic map of the study area, showing major normal faults, earthquake-related ruptures and macroseismical features associated with the 1861 Eliki (modified after Schmidt, 1879) and 1995 Egion earthquakes (data from Koukouvelas and Doutsos, 1996). Inset shows the five named normal faults south of Egion, on the southwestern shore of the Gulf of Corinth.

fact includes a number of smaller normal faults, has the most prominent fault scarp over the western part of the Gulf of Corinth. The Eliki fault scarp occurs in fan deltas and alluvial sediments in the east and fluviolacustrine and fluvial sediments in the west (Piper et al., 1990), and separates a well-defined WNW-trending range-front from the western part of the Gulf of Corinth graben. On the other hand, the 12-km-long Egion fault and its offshore extension affect the Egion area's coastal geomorphology (Koukouvelas, 1998b), and thus the fault is important for understanding the Quaternary evolution of the study area. The structural relationship of the two normal faults produces a transfer zone that down-flexes the area between them to the east (Roberts and Jackson, 1991; Koukouvelas, 1998a) (Fig. 2). Transfer zone deformation has resulted in the shifting of the Selinous river bed to the southeast at a rate of 15°/ka (Koukouvelas, 1998a). Both faults are characterized by high levels of seismic activity, and macroseismic data during historic events suggest that the Eliki and Egion normal faults may have hosted at least five strong earthquakes (Mouyaris et al., 1992; Koukouvelas and Doutsos, 1996; Stewart, 1996; Papazachos and Papazachou, 1997) (Fig. 1c).

3. The Eliki fault

3.1. Earthquakes related to the Eliki fault

Three strong earthquakes that may be related to reactivation of the Eliki fault are the events of 373 BC, AD 1402 and 1861 (Mouyaris et al., 1992). However, it is important to note that it is difficult to assign a given earthquake to a particular fault even with modern data (see Bernard et al., 1997) and that there are insufficient data to support the relation of the 1402 event with the Eliki fault (Mouyaris et al., 1992).

Aristotle, Eratosthenes and Herakleides in Strabo, Diodoros of Sicily, Strabo, Pausanias, Ovid, Pliny and Aelian described the macroseismic features associated with the 373 BC earthquake (Soter and Katsonopoulou, 1998). Although premonitory animal behaviour, as well as macroseismic anomalies during this earthquake, suggest that the earthquake affected an elliptical area along the shore about 30 km long, there is no mention of surface rupture during this earthquake (Papazachos and Papazachou, 1997; Soter, 1999). Similarly, only macroseismic features are known for the 1402 earthquake which caused severe damage from Xylokastron to Egion (Fig. 1c).

The 1861 Eliki earthquake was associated with a 13- to 15-km-long surface rupture (Schmidt, 1879) (Fig. 2). This rupture was concentrated along a prominent fault scarp and extended from the Pounta area in the east to Keryneia in the west. Vertical displacement up to 1 m is known for this event (Schmidt, 1879). The 1861 event produced extensive liquefaction in the coastal area (Schmidt, 1879) that can be directly compared with the 373 BC event (Marinatos, 1960) (Fig. 2). Surface ruptures associated with the 1861 event do not follow the whole length of the prominent Eliki fault scarp (Fig. 2). The surface rupture crosses the landscape to the west of the Kerynitis river, halting in an area of low relief east of Keryneia village, rupturing in essence only the eastern part of the fault (Fig. 2). The western part of the Eliki fault was not ruptured during the 1861 event. The two fault segments are thus separated by a persistent segment boundary, which can be called a 'salient' using, in a broad

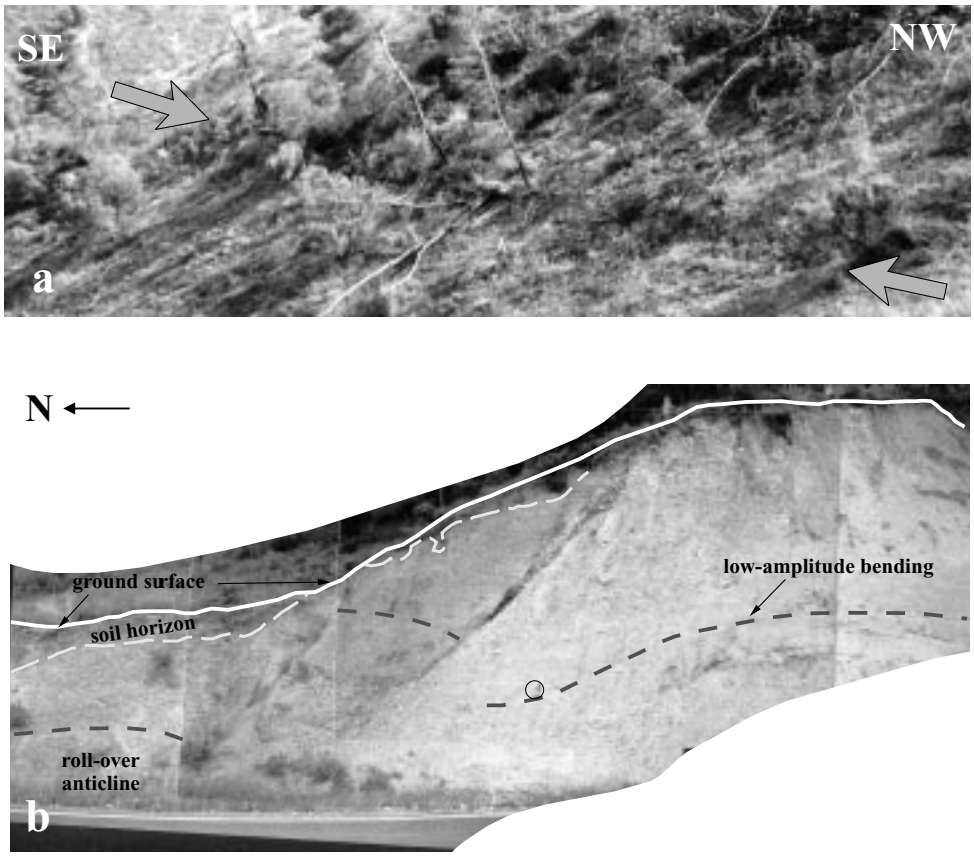

Fig. 3. (a) Photograph showing part of the surface rupture associated with the 1861 Eliki earthquake. Grey arrows highlight the trace of the rupture (for location, see Fig. 2). Width of photo: 100 m. (b) Photograph showing the southern end of the Eliki fault zone (for location, see Fig. 2). The two synthetic north-dipping faults define the lithological boundary between unconsolidated coarse-grained clastics and sandstones–conglomerates of Pliocene age. Note the progressive thinning of the soil horizon towards the fault, the roll-over anticline in the hanging wall and the low-amplitude buckling in the footwall. Width of photo-mosaic is 17 m, hammer for scale.

sense, the definitions of Machette et al. (1991). Of particular interest in terms of the role of fault segments during the earthquakes is the fact that the rupture was further separated into three step-type geometrical or structural segments (Fig. 2). The cross-strike distances between the en échelon steps of the rupture range from 0.6 to 1.5 km (Fig. 2). At both steps between the segments (Fig. 2), NE-trending ruptures were mapped by Schmidt (1879).

The geometry of the surface ruptures associated with the 1861 Eliki earthquake were similar to the surface ruptures associated with the 1995 Egion earthquake, although the two earthquakes appear to be related to different faults (Koukouvelas and Doutsos, 1996). Surface rupture associated with the 1995 Egion earthquake is defined by three left-stepping fault segments rupturing the east part of the fault. This surface rupture event was a typical extension-related earthquake characterized by small-scale co-seismic throw (for details, see Koukouvelas, 1998b). The following data suggest that the Egion fault was reactivated during the 1995 earthquake: (a) co-seismic offsets followed the geological throw and segmentation; (b) anomalous spring discharge was noted along the Egion fault trace before the 1995 Egion earthquake; (c) local pre-seismic surface movements were noted where co-seismic ruptures and warp-like hanging wall subsidence occurred near the fault's west end; (d) after-slip distribution doubled the co-seismic slip; (e) peak ground acceleration and damage concentration during the 1995 Egion earthquake event were strongly influenced by the Egion fault trace (Athanasopoulos et al., 1999). However, these data do not exclude the possibility that reactivation of the Egion fault affects the northern part of the Gulf of Corinth, as suggested by SAR interferometry (Bernard et al., 1997). This is because north-dipping faults in the Gulf of Corinth are rooted in a crustal scale decollement at a depth of 8–12 km, as suggested by geology and highlighted by seismology (see fig. 8 in Doutsos and Poulimenos, 1992; fig. 13 in Bernard et al., 1997). Furthermore, this analysis points to at least a qualitative relation between the two events in terms of geometrical similarities between the surface rupture pattern during the 1861 Eliki and the 1995 Egion earthquakes. Common characteristics are that the surface ruptures associated with these earthquakes were segmented along their strike. Step-over zones between the segments coincide with major changes in gross morphology, and along these steps co-seismic offset is diminishing.

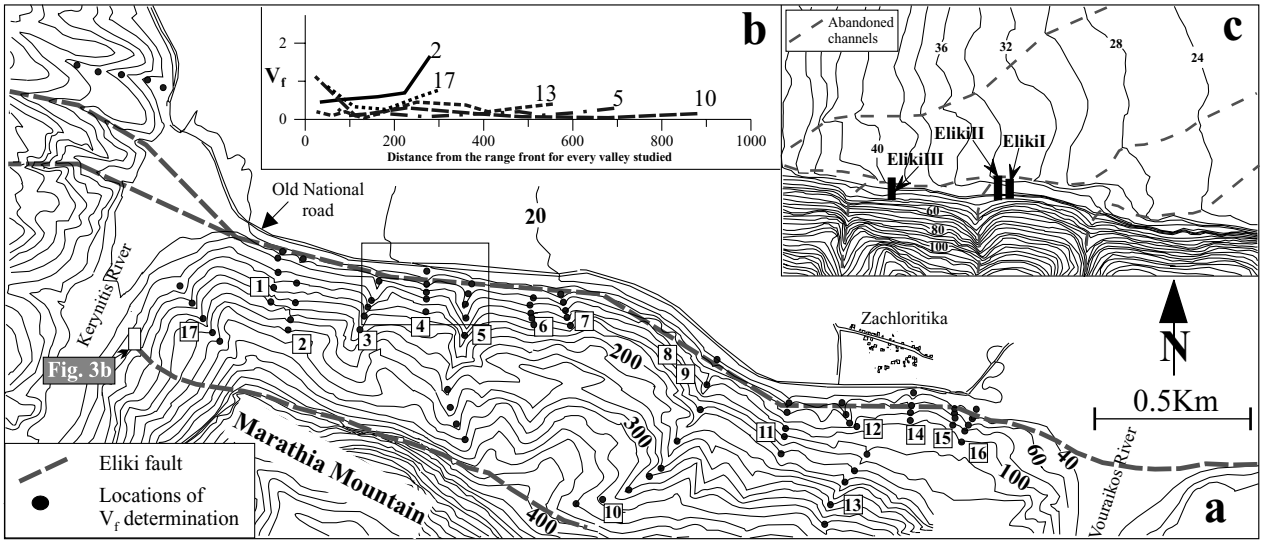

Fig. 4. (a) Morphotectonic map of the study area, showing the Eliki fault zone and drainage pattern across the fault scarp. Bold numbers show contouring at 100-m intervals and numbered boxes show streams draining the fault scarp. The rectangle shows the area of the detailed topographic map. (b) Diagram showing V_f data in the five longer streams draining the fault scarp. Numbers in the diagram correspond to the numbered streams on the morphotectonic map. (c) Detailed topographic map, contouring at 4-m intervals, showing the location of trenches as solid parallelograms and abandoned branches of the Kerynitis river as dashed grey lines.

Re-mapping of the 1861 Eliki earthquake rupture indicates additional differences between segments B and C. The former is a very linear trace while the later is more complex. Specifically, in the area between the Kerynitis river and the modern village of Keryneia, two parallel rupture strands appear to be associated with this earthquake. These are expressed as prominent 20- to 60-cm-high scarps affecting a zone about 120 m wide (Fig. 3a). This fits well with the rupture pattern in Schmidt's (1879) map, where the fault ruptures in this area are diffused in a zone. These ruptures are easily observed for 1.4 km west of the Kerynitis river and disappear in a steep valley (Fig. 2, heavy dot). Further west, the rupture is not well expressed and cannot be separated from present day small-scale landslides, or has disappeared due to cultivation. Furthermore, because the end of the rupture is less than 2.5 km from this area, it is possible that the co-seismic rupture offset was small and that prominent fault scarps are difficult to observe. A similar westward decrease in displacement along the surface ruptures was also observed during the 1995 Egion earthquake.

3.2. The footwall of the Eliki fault

The Eliki fault is a complex normal fault characterized by a composite fault scarp (sensu Stewart and Hancock, 1991). Detailed structural analyses of the Eliki fault between the Kerynitis and Vouraikos rivers suggest that two north-dipping and E–W-trending fault strands define the Eliki fault zone. One is located along the range front, and the second is a smaller fault 400 m to the south (Fig. 3b, and for location see Fig. 2). Between these two fault strands, six synthetic syn-sedimentary faults are recognized. In a road section, the southern fault strand splays into two synthetic faults and deforms the ground surface (Fig. 3b), producing a 5-m vertical offset defining the boundary between coarse-grained clastics and sandstone-conglomerate alternations. Detailed observations along this road section also indicate progressive thinning and disappearance of the present day soil horizon where the fault reaches the surface (Fig. 3b). This relationship, as well as fissures filled with soil in the footwall of this fault along a 3.5-m-high scarp, are interpreted to indicate recent reactivation of the fault (Fig. 3b).

The southern fault strand defines the headwater area of a series of small-scale streams draining the fault scarp (Fig. 4). Morphotectonic analysis of the impact of the Eliki fault on these small-scale rivers is defined by using the valley-floor width to valley height index, called V_f, following Bull and McFadden (1977). Using V_f, we can compare the index value with the tectonic activity along and across the Eliki fault zone. V_f is expressed by:

$$V_f = 2V_{fw}/[(E_{ld} - E_{sc}) + (E_{rd} - E_{sc})],$$

where V_{fw} is the width of the valley floor, E_{ld} and E_{rd} are the respective elevations of the left and right valley divides, and E_{sc} is the elevation of the valley floor. For the calculation of the ratio, we used a topographic map (1:5000) and all parameters are measured directly on this topographic map (also see Koukouvelas, 1998b). The calculation of the V_f factor over the footwall area is based on 17 small-scale streams with lengths ranging from 50 to 500 m between the Vouraikos and Kerynitis alluvial rivers (Fig. 4a). The streams are ephemeral and cross the Eliki fault zone at high angles. In these small-scale rivers, we analyse the ratio between the incision and the widening of the streams. For the purposes of this work, we present the V_f data in the

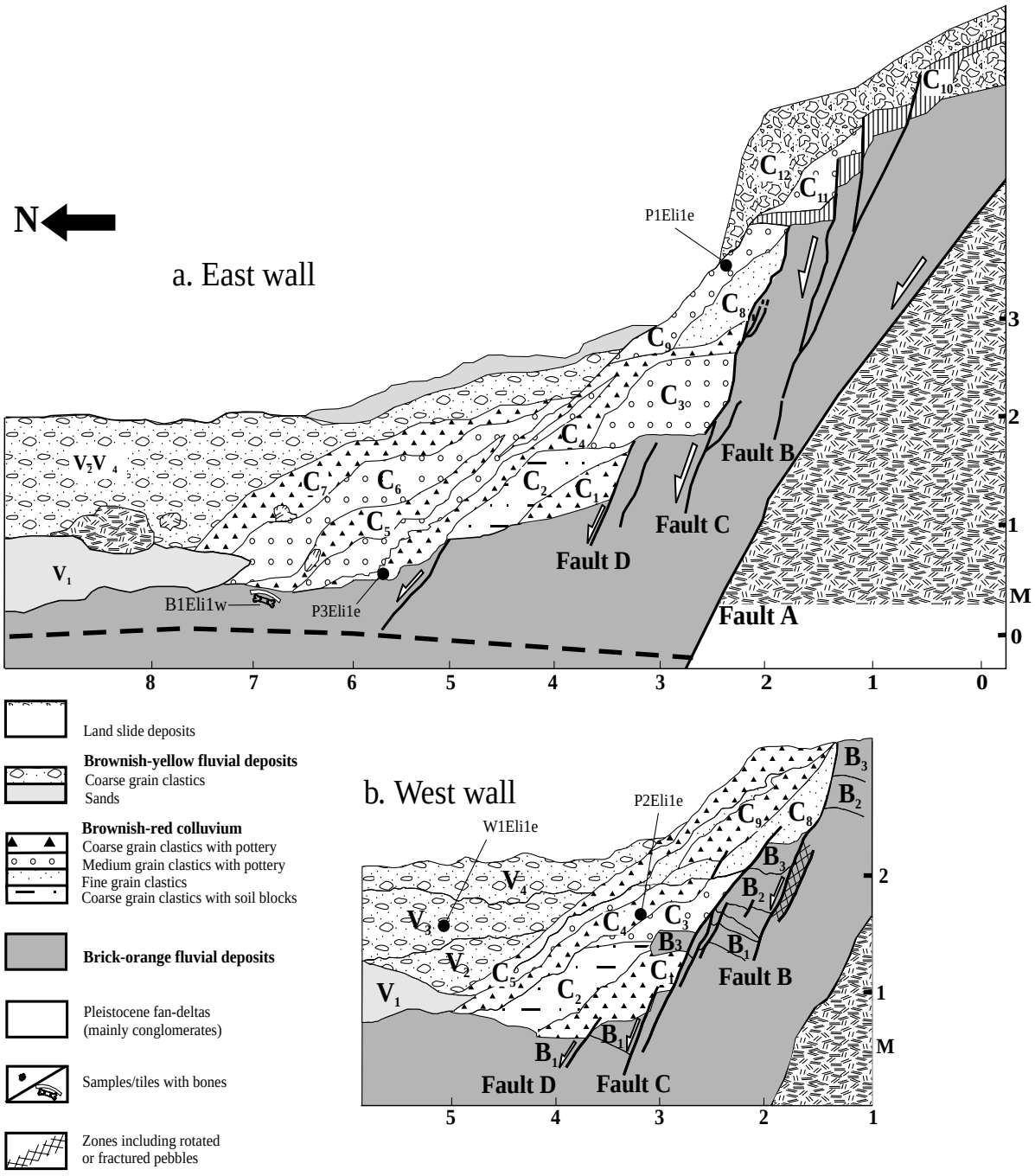

Fig. 5. Log of the trench Eliki I, initial mapping 1:20. The west wall is flipped. Dashed line shows the roll-over anticline.

five longer streams that are used as representative for understanding the tectonic activity over the fault zone. V_f for the five streams ranges between 0.1 and 2.0 in the footwall area of the Eliki fault scarp, showing predominantly down-cutting to lateral cutting (Fig. 4b). The V_f ratio along the fault shows low values close to the prominent fault scarp and higher values at the southern fault strand. This is interpreted as a quantitative index showing that the entire fault zone appears to be active in terms of the down-cutting stream activity. However, low values of V_f closer to the prominent fault relative to higher V_f values to the south indicate that, 200 m south of the front, the tectonic base level fall becomes progressively less significant, although the low values suggest a broad active fault zone.

4. Site stratigraphy

Three trenches were excavated in an area that, according to Schmidt's map (1879), was ruptured during the 1861

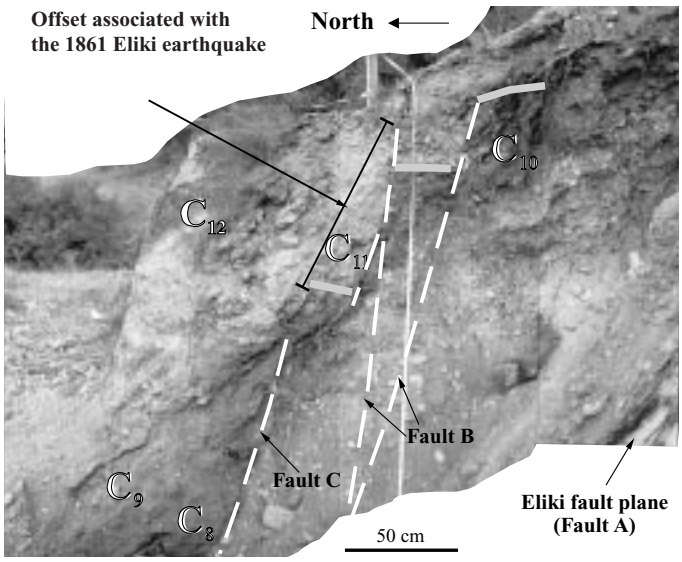

Fig. 6. Offset associated with the 1861 event as observed in the east wall of the Eliki I trench. Labeling C8–C12 corresponds to layers in the Fig. 5 (for explanations see text).

event. The trenches were excavated across the fault scarp, and their walls were logged in detail (scale 1:20). Trench Eliki I (Fig. 4c) was chosen for further analysis because it exhibits multiple faulting events with clear displacements, consequent development of colluvium and the presence of datable materials (i.e. charcoal, pottery fragments and human bones) (Fig. 5). The trench exposed bedded, coarse fluvial and colluvial sediments and buried soils, and is analysed in detail.

In general, each Eliki fault reactivation is followed by deposition of scarp-derived laterally accreted colluvium that interfingers with vertically accreted fluvial deposits; these two types of deposits bury older, brick-orange alluvial deposits at the base of the trench.

The oldest deposit in the trench is a coarsening upward, brick-orange fluvial formation. Adjacent to the fault at the southern end of the trench, this deposit includes imbricated coarse-grained pebble and cobble conglomerate (Fig. 5a, layers B1–B3). Pebbles and cobbles of these layers are imbricated. In a 10-cm-wide rubble zone (Fig. 5b), the long axes of those pebbles are rotated toward the maximum dip direction of fault B or are fractured by the fault. Away from the fault scarp, this fluvial formation consists of thin-sand and sandy-clay strata, alternating with cross-stratified sand lenses and channel deposits. The upper surface of the brick-orange deposit is cemented by pedogenic calcium carbonate (caliche), suggesting an erosional upper surface or a soil horizon. Caliche usually develops in flat flood plain environments, and thus we speculate that, during the period corresponding to the caliche segregation, the top of the brick-orange formation was almost flat. These observations suggest that the brick-orange fluvial deposits constitute an overbank sedimentary environment, which is commonly exposed in the Peloponnesus (see Piper et al., 1976). This older fluvial unit is flat lying away from the fault and dips to the south close to the fault, thus forming a rollover anticline (Fig. 5a).

The brick-orange formation is systematically covered by the brownish-red series of the accreting colluvium (Fig. 5). The colluvium series is separated into three colluvial wedges. The upper one is controlled by the fault strand B and includes the layer C11 corresponding to the 1861 event. The stratigraphically lower colluvium wedge controlled by the fault strand C includes the layers C3–C4 and the layers C8–C9. Finally, the lower one controlled by the fault strand D includes the layers C1–C2 (Fig. 5a). The colluvium includes poorly sorted pebble or cobble conglomerates in a brown to reddish sandy matrix, thin interbedded palaeosols and conglomerate blocks interpreted to have been derived from the free face (Fig. 5). In the upper part of the colluvium, curved palaeosol horizons are interpreted as the result of soil creep. The existence of large clasts and intact blocks of soil horizons (i.e. layers C2 and C6) in the colluvium suggests that this represents a debris facies of a proximal colluvial wedge (sensu Nelson, 1992).

The colluvium also includes tile fragments, human bones, and two layers rich in charcoal and pottery fragments (Fig. 5, layers C5 and C7). Individual layers in the colluvial deposits thin towards the fault and dip moderately to the north at a mean angle of 41°, which is the typical repose angle for recent screes in the area. The overall geometry of the colluvial wedge suggests that the colluvium, which masks the brick-orange formation, is the result of fault reactivation. The upper layer of the colluvium is a coarse grained unsorted conglomeratic layer including conglomerate blocks. Based on the absence of sorting, we interpret this layer of the colluvium as a partly preserved landslide deposit attaining a maximum thickness of 1.3 m and burying the scarp associated with the 1861 event (Figs. 5 and 6). Much of the section's upper part

Table 1
Showing sample description and ages

Sample No.	Layers/ description	Dating method	Age in YBP/2σ
P1Eli1e	C12/pottery	TL	745±56
P2Eli1e	C4/pottery	TL	1079±85
P3Eli1e	C3/pottery	TL	2049±150
W1Eli1e	V3/wood fragment	C14	300±120
B1Eli1w	B1/bone	C14	3020±880

P1-P3 samples dated by Institute of Geology and State Seismological Bureau, Beijing, China.
W1, B1 samples dated by the University of Georgia, Athens, US.
YBP = years before present.

corresponds to a wash facies, and is missing due to recent cultural disturbances.

Interfingering with the colluvium and covering the brick-orange formation in the trench are vertically accreting fluvial deposits of the basin. The fluvial deposits include a sequence of thin-bedded sandy layers that cover the horizontal parts of the older formation and four coarse-grained layers, each of which interfinger with the colluvial deposits (Fig. 5a, layers V1–V4). These contact relationships suggest that the colluvium and the fluvial formation are two formations that accumulated coevally. The four coarse-grained layers that cover the colluvium have their maximum thickness at the base or nearby the fault scarp (Fig. 5, layers V1–V4). The lower of these layers includes rapid alternations of clay sand, mud and gravel layers. This layer is separated by an erosional surface from a clast-supported unconsolidated fresh-water layer attaining a maximum thickness of 0.5 m close to the fault trace and rapidly diminishing basinwards (Fig. 5, west wall layer V2). This layer is covered by a basinward thickening debris flow attaining a maximum thickness of 0.62 m (Fig. 5, west wall layer V3). Finally, the upper layer of this formation is another debris flow deposit that attains a maximum thickness of 0.44 m close to the fault scarp (Fig. 5, west wall layer V4). On top of the last debris flow layer there is a thin palaeosol up to 12 cm in thickness (Fig. 5a).

In the Eliki I trench, we collected three tile fragments for thermoluminence dating. We also collected two fragments of human bones, probably coming from a tile-covered Roman grave (for details, see Section 6), and a wood fragment for ^{14}C dating (Fig. 5, Table 1).

5. Events interpreted from trench exposures

The brick-orange formation, the oldest formation exposed in the trench, is continuously buried by the colluvial units and is thus used as a reference horizon for the structural analysis. Furthermore, its internal stratigraphy is detailed enough for lithological correlation and its upper surface, which was almost flat, is offset into discrete steps. Thus, these vertical displacements are used for the resolution of co-seismic deformation.

The Eliki Fault is exposed in all excavated trenches as a fault zone affecting the unconsolidated sediments. In particular, the fault zone exposed in the Eliki II trench attains its maximum observed width of about 8 m, whereas in the Eliki I trench, the width is only 5.2 m (Fig. 4c). This difference in fault zone width is interpreted as due to two possible causes: (a) the fault displacement diminishes rapidly towards the west as fault slip is transferred to the main fault zone 15 m to the north or (b) the fault zone in the Eliki I trench attains the maximum width at a shallower depth due to eastward thickening of the sediments. The fault zone in the Eliki I trench includes three faults splaying off of the primary fault (fault A) that is exposed in the southern end of the trench. Thus, the fault movement produces a composite fault scarp. The splays are synthetic to the main fault, are spaced about 1 m apart and have an average dip of 60°. Given that the main fault dips to the north at about 50°, these splays probably merge with the main fault just below the base of the trench. This suggests that most of the events on the Eliki fault rupture the same part of the fault zone.

At the southern end of the trench, the fault zone is exposed as a north-dipping striated plane, across which Pliocene–Pleistocene conglomeratic fan-delta deposits are vertically offset more than 400 m. The fault zone in the unconsolidated deposits vertically displaces the orange-brick formation downwards to the basin by a cumulative stratigraphic offset of 3.4 m. This slip displacement discontinuity is interpreted as the result of three discrete events.

Table 2
Minimum displacements (cm) of events through Eliki I

	Stratigraphic offset[a]	Vertical displacement or throw[b]	Horizontal displacement or heave[b]	Estimated magnitudes (M)[c]
Event 1	105	93	50	6.7
Event 2	179	137	117	6.8
Event 3	52	44	33	6.5
Total displacement	**336**	**273**	**200**	

[a] Stratigraphic offset measured directly in the trench.
[b] Throw and heave are calculated from the vertical separation of a layer and the directly measured displacements.
[c] Moment magnitude estimations based on empirical relationships of Pavlides et al. (2000).

The following displacement estimates contain uncertainties related to the erosion of scarps and human activities in historical times, and thus the estimates should be considered as minima (Table 2).

Event 1, the 1861 earthquake, produced a total vertical displacement of 0.93 m that occurred mainly on the first splay (Fig. 5, east wall fault B) spaced 1 m from the main fault (Fig. 6). Close to the surface, this offset is distributed in a series of synthetic ruptures. The fault scarp is then buried by the colluvial layer C11. In the same area, Schmidt's (1879) measurements suggest 1 m of vertical offset and, if we accept this measurement as accurate, then probably the erosion of the fault free face produces the 7% deficit. Event 2 is defined by the offset of the layer B3 in the second fault splay down to the basin by 1.37 m and is related to the formation of two colluvial wedges (Fig. 5). The wedges are vertically accreted and include layers C3–C4 and C8–C9. The colluvium layers C3 and C4 bury the lower half of the fault scarp associated with this event that has produced the offset of the layer B3. However, it is important to note that it is difficult to define if the B3 in the west wall was deposited above the colluvial layers C1–C2 or the B3 is a block from the free face sliding on the top of C1–C2. Thus, the present analysis cannot distinguish whether the layers C3–C4–C8–C9 composing the colluvial wedge were produced by one or two events. Therefore, either the pre-1861 event produced a vertical displacement of 1.37 m or there were two events, the first of which produced a vertical displacement of 0.44 m followed by a second event associated with 0.93 m offset. We will accept the hypothesis of one event trying to correlate every step of the brick-orange formation with an event, and thus hereafter we will interpret the pre-1861 event as having produced a vertical displacement of 1.37 m.

Event 3 is defined by the vertical displacement of the horizon B1 by 0.44 m, and the colluvium layers C1–C2 subsequently buried the fault scarp produced by this event. Event 3 in the section is observed on the two fault splays and offset the layer B1 in a step-like manner (Fig. 5b).

6. Archaeological data

We describe here a set of archaeological data because this will provide the basis to understand dating results which will be presented below. Among the debris of the excavated strata of the trench, we noticed several ancient fragments of curved, well-fired clay tiles of light brown colour. One of the fragments had an attached lump of earth of yellowish brown colour in its interior side, the humus containing fragments of a long bone, probably from a human skeleton (Fig. 5a, Table 1).

Closer observation of both faces of the excavated trench revealed fragments of similar tiles exposed on the western face of the trench at a depth of about 3 m from the surface. The layer containing the tile fragments is located at the upper part of the brick-orange formation (Fig. 5). According to archaeological evaluation, the fragments probably come from a tile-covered grave built with clay roof tiles, placed lengthwise, with an E–W direction. The tomb was probably constructed with at least two successive layers of tiles, as indicated from samples which preserve fragments of two tiles bound together with whitish stucco. Judging from the shape, the thickness and the lack of paint on both sides of the tiles, we infer that the grave should be dated to the Roman period. Tile-covered graves are known from Archaic times (600–480 BC), become more common in the Classical period (480–323 BC), and are very typical of Hellenistic times and later (323 BC onwards) (Kurtz and Boardman, 1971). In our case, the unpainted light brown tiles suggest a Roman date for the grave. The possible presence of a Roman tomb at a depth of 3 m below the surface in this site well agrees with the discovery of buried Roman occupation horizons in the major Helike area, including our Eliki I trench site, during work conducted by the Helike Project in the last 10 years (Soter and Katsonopoulou, 1998). More specifically, the first excavation carried out in the Helike area (Klonis field) under the direction of D. Katsonopoulou brought to light a large Roman building buried about 1.5 m below the surface at this part of the plain (Katsonopoulou, 1998).

Given the possible presence of a Roman grave in the Eliki I trench, further investigation of this site would in all probability provide additional archaeological data that will enable us to reconstruct in detail the palaeotopography of this significant site along the Eliki fault scarp. Based on the data available so far, we can suggest that the Eliki I trench is located at the base of a prominent fault scarp, where a cemetery probably existed during ancient times, its existence suggesting that the top of the brick-orange formation was more or less flat and was an occupation horizon archaeologically dated to the Roman period.

7. Dating the events in the trench

From the Eliki I trench, five stratigraphically consistent ages are available (Table 1), enabling the timing of events. However, before describing the radiocarbon analyses and the thermoluminence results for dating events, we need to discuss the samples B1Eli1w and P3Eli1e. These two samples, collected from the top of the brick-orange formation and the base of the colluvium, define the onset of the colluviation. Also, most of our archeological data come from the description of the tile-covered grave and thus the age of the bones is very important for understanding the colluvium tectonostratigraphy. The dated bone sample had a weight of 35 g, and after the removal of the interstitial carbonates the remaining material gave an age of 3020 ± 880 AD. This error interval can be reduced by using archaeological evidence showing that the grave was

probably between Late Hellenistic and Roman in age. Thus, the age that corresponds to the onset of the colluviation is probably close to 100 BC, so the time interval represented by the stratigraphy encountered in the trench is later than 373 BC.

The upper part of the Eliki I trench is characterized by an offset of layer C10 by 0.93 m. The C10 layer contain less than 10% carbon material and can be classified as the A horizon. We interpret this event as younger than the pottery fragment P1Eli1e (Fig. 5, layer C9). Pottery fragments in the layer C9 are recognized as Ottoman and their thermoluminence date is 1200–1311 AD (Table 1, sample P1Eli1e). Thus, based on this date and the fact that the offset is the latest in the fault and the closest to the surface, we suggest that this event is the well-known 1861 Eliki earthquake. In the Eliki II trench, the same event is observed in the southern end of the section, where the sedimentation onlaps fan delta deposits. In this trench, the 1861 rupture may have formed two strands, one as a 0.5-m-high permanent scarp affecting the landscape while the rest, with about 0.4-m offset, is recognized by the offset of fan-delta conglomerates. We interpret event 2 to be older than the pottery fragment P2Eli1e (upper part of the layer C4) and younger than P3Eli1e (lower part of the layer C4). In these two pottery fragments in layer C4, we have thermoluminence dates of 190 BC–110 AD and 836–1106 AD, respectively. This suggests that event 2 (or events?) occurred in the interval 190 BC–1311 AD. Given the absence of more data, we suggest that the most probable age is close to the middle of this period, 600 AD. Further evidence for an event close to this period comes from radiocarbon dating of an emergent notch (>1.5 m high) east of Diakopto, between 440 and 870 AD (Stewart, 1996). We interpret event 3 to be older than the pottery fragment in the lower part of layer C4 (Table 1, sample P3Eli1e) dated at 190 BC–110 AD and younger than the bones in layer B1 (Table 1, B1Eli1w). For the bones we use an age that is compatible with the ^{14}C dating, and the archaeological dating of the tile fragments, which suggests a most probable age close to 100 BC. This implies that event 3 occurred in the time interval between 100 BC and 110 AD, with the most probable age close to the middle of this period.

We recognized two severe flooding events in the Eliki I trench (Fig. 5, west wall layers V3 and V4) and an open framework layer V2, which attain their maximum thickness close to the fault scarp and appear to be related to the back-tilting of the fault's hanging wall. We interpret the first flooding event as being younger than the charcoal fragment (Table 1, sample W1Eli1e) in layer V3, dated at 1697–1710 AD. However, sedimentary structures in these debris flows suggest an eastward flowing stream and thus probably the river branch belongs to the Kerynitis river (Piper, D.J.W., personal communication, 1999). This relationship suggests that the renewed faulting (events 1 and 2) may have created or increased the topographic depression all along the fault zone, enabling climatically controlled flooding events to discharge through a river branch parallel to the fault during the period between the second event and the present day. This renewed topographic depression also implies a rise in the groundwater level, as suggested by the red–brown colour of the colluvium (also see Kontopoulos and Stamatopoulos, 1990).

In the present day, abandoned channels on the Kerynitis alluvial plain suggest that co-seismic subsidence probably triggers the reactivation of abandoned channels (Fig. 4, inset) and produces small-scale deltas. Similar river branches producing small-scale deltas are well known for the contemporary Selinous, Vouraikos and Kerynitis rivers. The Kerynitis river presently bends to the northwest after crossing the Eliki fault, and this shifting is also shown on the Venetian maps of 1700 (Dokos and Panagopoulos, 1993). Both the Selinous and Kerynitis rivers drain to Nikoleika bay, the area that showed the highest co-seismic subsidence and liquefaction during the earthquakes of 373 BC, 1861 and 1995.

Summarizing these data, in the Eliki I trench we know of a series of tectonic events in the interval of 100 BC–1861 AD and flooding events. Stratigraphic relationships suggest that the flooding events are correlated with the two younger seismic events, which had onlapping of a fault scarp, and with the concentration of most of the ceramic fragments and the bones. If we compare the offsets of these two events recognized in the Eliki I trench with the debris flow thicknesses, then flooding events in the study area are apparently correlated with subsidence and back-tilting. Thus, co-seismic offsets causing reactivation of abandoned channels may have been produced by the two younger events.

8. Slip rate over the western part of the Gulf of Corinth

Age data and offsets in the trench indicate that three events in a time interval of about 2000 years produced a total stratigraphic offset of about 340 cm, which can be separated into 273 cm of vertical displacement or throw and 200 cm of extension or heave. These estimates indicate that the minimum vertical displacement and extension accommodated by the fault are as much as 1.4 and 1 mm/year, respectively. The location of the trench at the centre of the Eliki fault suggests that these estimations should be the largest along the fault. Indeed, our co-seismic slip rates are significantly higher than the estimations in the Diakopto area, which is located at the eastern end of the Eliki fault (Stewart and Vita-Finzi, 1996). In the Diakopto area, dating of the emergent notches suggests co-seismic uplift of the order of 0.25 mm/year. Furthermore, in order to extrapolate uplift into slip rate, we consider the case for the Egion fault, where the uplift/subsidence ratio is 1:2 (Koukouvelas and Doutsos, 1996), and therefore we postulate that the slip rate in the eastern end of the Eliki fault is of the order of 1 mm/year.

Slip rate estimates for the Egion fault based on the co-seismic displacement during the 1995 Egion earthquake and the 107 years elapsed from the previous earthquake suggest that the amount of vertical displacement is about 0.7 mm/year, while its extension accommodated by the fault is as much as 0.5 mm/year (for details regarding recurrence interval for the Egion fault, see Koukouvelas, 1998b). We assume that these estimates are also realistic for longer time intervals, based on geological data (Doutsos and Poulimenos, 1992; Koukouvelas and Doutsos, 1996). As those two faults are parallel to one another, and their slip vectors are almost perpendicular to the fault trace (Roberts and Koukouvelas, 1996), they accommodate about 10% of the geodetically measured total extension of 13 mm/year over the study area (Clarke et al., 1998). As these two faults are known to be seismically active, and the geodetic data suggest a much higher extension rate in the area (see Clarke et al., 1998), we suggest that other faults in the area are also important. Indeed, in this area, a series of three onshore normal faults and two offshore faults that are spaced 2–4 km apart are associated with significant geological displacements (Doutsos and Poulimenos, 1992) (Fig. 1c). If these other faults slip at the rate of the Eliki fault, then the total extension rate increases to a value that is only 50% of the geodetically estimated extension. However, based on sediment thickness and geomorphological data, the three onshore normal faults are less active than the Eliki fault.

9. Discussion

The palaeoseismological and archaeometric data (^{14}C dating of bone fragments, ^{14}C dating of wood and thermoluminence dating of tile fragments), combined with the archaeological data, suggest that the Eliki I trench probably occupies the site of a cemetery. In addition, the existence of Roman tiles coming from a tile-covered grave, located about 3 m below the surface, suggests that occupation corresponds to the level of the old alluvial plain during the Late Hellenistic–Roman period.

We can define the same lithological succession in both the Eliki I and II trenches, although pottery and bones are missing in the western one. The absence of pottery and bones is due to the fact that the Eliki II trench is close to the exit of a small gully in the alluvial plain. This succession starts with nearly horizontal strata 8 m from the fault scarp or at the deeper part of the Eliki I trench and is progressively back-tilted close to the fault. The two debris-flow horizons attain maximum thickness close to the fault scarp, probably due to the renewed back-tilting of the Eliki fault hanging wall, which reactivated abandoned channels of the Kerynitis river parallel to the fault scarp. At present, this river has shifted westwards due to the combined effect of both the Eliki and Egion faults on the Kerynitis–Selinous alluvial plain (also see Koukouvelas, 1998a). Northwestward shifting and the abandonment of eastward-flowing deltaic branches of the river are known to have been prominent at least before 1700. Thus, we can infer that the two younger events produced a vertical displacement of about 2.5 m that was critical for the vertically accreted basin deposits. Therefore, these two flood events are constrained between 1700 and the present, with a recurrence interval of 150 years. These two flood layers mask the scarp and the colluvium wedge by about 1.5 m. Of particular interest for the interpretation of these trenches is the fact that the lithofacies thicken eastwards, suggesting that the same events are at different depths in the two sections. This rapid change of the fault zone width is also observed in the Pisia–Skinos fault zone trenches in the eastern Gulf of Corinth (Collier et al., 1998).

Colluvium tectonostratigraphy in the Eliki I trench suggests fault-controlled sedimentation along with vertical displacements ranging from 0.44 up to 1.37 m. The particular features of the last offsets in the Eliki I section indicate splaying into second-order faults of an almost continuous fault at depth. This style of deformation is similar to the observed co-seismic ruptures in other earthquakes and active normal faults in the Peloponnesus (Stewart and Hancock, 1991; Koukouvelas et al., 1996).

Of particular interest for the palaeoseismicity of the Eliki fault is also the fact that the two younger events are related to 0.93 and 1.37 m of throw, while the older event is related to much smaller throw of 0.44 m. All trenches are excavated in the middle of the Eliki fault (Fig. 2) and thus we can reasonably assume, even it is known that co-seismic displacement varies along strike, that co-seismic displacements in our trench are probably close to the largest offset. From these suggestions, the mean value of the magnitude estimate is derived using the empirical relationship of Pavlides et al. (2000) for maximum displacement and M_s:

$$M_s = 0.64\log D + 6.76.$$

Thus, the earthquakes interpreted from the trench exposures, given the uncertainties in estimating the offset, are moderate in magnitude, ranging between 6.5 and 6.8. Finally, if we take into account the 373 BC penultimate event, which is probably of greater magnitude than the 1861 event (also see Stewart, 1996; Soter, 1998), then the seismic behaviour appears to be variable through time, producing vertical displacements ranging between 0.44 and 1.37 m.

10. Conclusions

(1) Palaeoseismological trenching and fault colluvial tectonostratigraphy indicate that the Eliki fault is related to three earthquake events over a period of 2000 years. These events are double the number of events known from historical seismicity archives. Recurrence intervals for these events, as well as the 373 BC event, are estimated to range between 270 and 1200 years.

(2) The trench stratigraphy indicates that there is no evidence supporting the characteristic earthquake model, but an overall variable through time seismic behaviour, producing vertical displacements ranging between 0.44 and 1.37 m, during moderate magnitude events.

(3) The slip rate on the fault over the past 2000 years is estimated at about 1.5 mm/year, while the extension accommodated by the Eliki fault is about 1 mm/year. These rates, combined with the strain relaxation produced by the Egion fault, suggest that these two faults accommodate about 10% of the present day extension in the area.

Acknowledgements

We would like to thank T. Doutsos for continuous encouragement and discussions, D.J.W. Piper for suggestions concerning the colluvium tectonostratigraphy of the trenches, S. Soter for field discussion and constructive comments on earlier versions of the manuscript, and T. Rockwell for discussions on the interpretation of events from trench exposures. We also thank R. Collier and D. Panstosti for making comments on an earlier version of the manuscript, and discussing events and stratigraphy in the trench. D. Pyrgakis helped with the fieldwork and drafting of Fig. 3. I.K.K. thanks the Rock Fracture project, Department of Geological and Environmental Studies, Stanford University, for hospitality while this work was completed. The editing assistance of J. Turner and the constructive reviews of two anonymous referees greatly improved the manuscript.

References

Ambraseys, N.N., Jackson, J., 1990. Seismicity and associated strain of central Greece between 1890 and 1988. Geophysical Journal International 101, 663–708.

Athanasopoulos, G.A., Pelekis, P.C., Leonidou, E.A., 1999. Effects of surface topography on seismic ground response in the Egion (Greece) 15 June 1995 earthquake. Soil Dynamics and Earthquake Engineering 18, 135–149.

Bernard, P., et al., 1997. The Ms = 6.2, June 15, 1995 Aigion earthquake (Greece): results of a multidisciplinary study. Journal of Seismology 1, 131–150.

Billiris, H., et al., 1991. Geodetic determination of tectonic deformation in central Greece from 1900 to 1988. Nature 350, 124–129.

Bull, W.B., McFadden, L.D., 1977. Tectonic geomorphology north and south of the Garlock Fault, California. In: Doehring, D.O. (Ed.), Geomorphology in Arid Regions: Annual Binghamton Conference. State University of New York at Binghamton, pp. 115–136.

Chatzipetros, A., Pavlides, S., Mountrakis, D., 1998. Understanding the 13 May 1995 Western Macedonia Earthquake: a paleoseismological approach. Journal of Geodynamics 26, 327–339.

Clarke, P.J., et al., 1998. Crustal strain in central Greece from repeated GPS measurements in the interval 1989–1997. Geophysical Journal International 135, 195–214.

Collier, R.E., Leeder, M.R., Rowe, P.J., Atkinson, T.C., 1992. Rates of tectonic uplift in the Corinth and Megara basins, central Greece. Tectonics 11, 1159–1167.

Collier, R.E., Pantosti, D., D'Addezio, G., DeMartini, P.M., Masana, E., Sakellariou, D., 1998. Paleoseismicity of the 1981 Corinth earthquake fault: seismic contribution to extensional strain in central Greece and implications for seismic hazard. Journal of Geophysical Research 103, 30001–30019.

Crone, A.J., Omdahl, M.E., 1987. Direction in paleoseismology. USGS, Proceedings Conference XXXIX, Open-File report 87-637.

Dokos, K., Panagopoulos, G., 1993. The Venetian Land Registry of Vostitsa. Educational Institute Agricultural Bank of Greece, Athens.

Doutsos, T., Piper, D.J.W., 1990. Listric faulting, sedimentation, and morphological evolution of the Quaternary eastern Corinth rift, Greece: first stages of continental rifting. Bulletin of the Geological Society of America 102, 812–829.

Doutsos, T., Poulimenos, G., 1992. Geometry and kinematics of active faults and their seismotectonic significance in the western Corinth–Patras rift (Greece). Journal of Structural Geology 14, 689–699.

Doutsos, T., Kontopoulos, N., Poulimenos, G., 1988. The Corinth–Patras rift as the initial stage of continental fragmentation behind an active island arc (Greece). Basin Research 1, 177–190.

Guidoboni, E., 1994. Catalogue of Ancient Earthquakes in the Mediterranean Area up to the 10th Century. Instituto Nationale di Geophysica, Rome.

Jackson, J.A., 1994. Active tectonics of the Aegean region. Annual Review of Earth and Planetary Science Letters 22, 239–271.

Jackson, J., 1999. Fault death: a perspective from actively deforming regions. Journal of Structural Geology 21, 1003–1010.

Jackson, J.A., McKenzie, D.P., 1988. Rates of active deformation in the Aegean Sea and surrounding areas. Basin Research 1, 121–128.

Jackson, J.A., Gagnepain, J., Houseman, G., King, G.C.P., Papadimitriou, P., Soufleris, C., Vireux, J., 1982. Seismicity, normal faulting, and the geomorphological development of the Gulf of Corinth (Greece): the Corinth earthquakes of February and March 1981. Earth and Planetary Science Letters 57, 377–397.

Kahle, H.G., Straub, C., Reilinger, R., McClusky, S., King, R., Hurst, K., Veis, G., Cross, P., 1998. The strain rate field in the eastern Mediterranean region, estimated by repeated GPS measurements. Tectonophysics 294, 237–252.

Katsonopoulou, D., 1998. The first excavation at Helike: Klonis field. In: Katsonopoulou, D., Soter, S., Schilardi, D. (Eds.), Ancient Helike and Aigialeia. Proceedings of the Second International Conference, Aigion, December 1995, pp. 125–145.

Kontopoulos, N., Stamatopoulos, L., 1990. A stream-flow controlled "wet" late Quaternary alluvial fan, NW Peloponnese, Greece. Il Quaternario 3, 61–72.

Koukouvelas, I.K., 1998a. Transfer zones along active normal faults in Peloponnesus, Greece. Bulletin of Geological Society of Greece 32, 221–229.

Koukouvelas, I.K., 1998b. The Egion fault, earthquake-related and long-term deformation, Gulf of Corinth, Greece. Journal of Geodynamics 26, 501–513.

Koukouvelas, I.K., Doutsos, T., 1996. Implication of structural segmentation during earthquakes: the 1995 Egion earthquake, Gulf of Corinth, Greece. Journal of Structural Geology 18, 1381–1388.

Koukouvelas, I.K., Mpresiakas, A., Sokos, E., Doutsos, T., 1996. The tectonic setting and ground hazards of the 1993 Pyrgos earthquake, Peloponnese, Greece. Journal of the Geological Society of London 153, 39–49.

Koukouvelas, I.K., Asimakopoulos, M., Doutsos, T., 1999. Fractal characteristics of active normal faults: an example of the eastern Gulf of Corinth, Greece. Tectonophysics 308, 263–274.

Kurtz, D., Boardman, J., 1971. Greek Burial Customs. Thames & Hudson, London.

Le Pichon, X., Chamot-Rooke, N., Lallemand, S., Noomen, R., Veis, G., 1995. Geodetic determination of the kinematics of central Greece with respect to Europe: implications for eastern Mediterranean tectonics. Journal of Geophysical Research 100, 12675–12690.

Machette, M., Personius, S.F., Nelson, A.R., Schwartz, D.P., Lund, W.R.,

1991. The Wasatch fault zone, Utah—segmentation and history of Holocene earthquakes. Journal of Structural Geology 13, 137–149.

Marinatos, S.N., 1960. A submerged town of classical Greece. Archaeology 113, 186–193.

McCalpin, J.P., 1996. Paleoseismology in extensional tectonic environments. In: McCalpin, J.P. (Ed.), Palaeoseismology. Academic Press, New York, pp. 85–146.

Mouyaris, N., Papastamatiou, D., Vita-Finzi, C., 1992. The Helice fault? Terra Nova 4, 124–129.

National Observatory of Athens, 1999. Seismicity Maps 1964–1999. http://www.gein.noa.gr/English/home-en.html.

Nelson, A.R., 1992. Lithofacies analysis of colluvial sediments—an aid in interpreting the recent history of Quaternary normal faults in the Basin and Range province, western United States. Journal of Sedimentary Petrology 62, 607–621.

Nur, A., Cline, E.H., 2000. Poseidon's horses: plate tectonics, earthquake storms in the Late Bronze Age Aegean and eastern Mediterranean. Journal of Archaeological Science 27, 43–63.

Papazachos, B.C., Papazachou, C., 1997. The Earthquakes of Greece. Edition Ziti, Thessaloniki.

Papazachos, C.B., Papaioannou, A.C., Papazachos, B.C., Savaidis, A.S., 1999. Rupture zones in the Aegean. Tectonophysics 308, 205–221.

Pavlides, S., 1996. First palaeoseismological results from Greece. Annali di Geophysica 39, 545–555.

Pavlides, S., Mountrakis, D., Kilias, A., Tranos, M., 1990. The role of strike-slip movements in the extensional area of Northern Aegean (Greece). A case of transtensional tectonics. Annales Tectonicae 4, 196–211.

Pavlides, B.S., Zhang, P., Pantosti, D., 1999. Earthquakes, active faulting, and paleo-seismological studies for the reconstruction of seismic history of faults. Tectonophysics 308, vii–x.

Pavlides, S., Chatzipetros, A., Caputo, R., 2000. Earthquake fault ruptures of the broader Aegean region as quantitative input to seismic hazard assessment. Active Fault Research for the New Millenium, pp. 371–375. Proc. Int. Symp., Hokudan, Japan, 17–26 Jan 2000.

Piper, D.J.W., Panagos, A.G., Kontopoulos, N., Pe, G.G., 1976. Deposition environments of Pliocene littoral sediments, Gythion, Southern Peloponnese, Greece. Zeitschrift der Deutschen Geologische Gesellschaft 127, 435–444.

Piper, D.J.W., Stamatopoulos, L., Poulimenos, G., Doutsos, T., Kontopoulos, N., 1990. Quaternary history of the Gulfs of Patras and Corinth, Greece. Zeitschrift fur Geomorphologie 34, 451–458.

Roberts, G.P., Koukouvelas, I.K., 1996. Structural and seismological segmentation of the Gulf of Corinth fault system: implication for models of fault growth. Annali di Geophysica 39, 619–646.

Roberts, S., Jackson, J., 1991. Active normal faulting in central Greece: an overview. In: Roberts, A.M., Yielding, G., Freeman, B. (Eds.), The Geometry of Normal Faults. Geological Society, London, Special Publication 56, pp. 125–142.

Schmidt, J., 1879. Studien uber Erdbeben. Carl Schottze, Leipzig, pp. 68–83.

Soter, S., 1998. Holocene uplift and subsidence of the Helike Delta, Gulf of Corinth, Greece. In: Stewart, I.S., Vita-Finzi, C. (Eds.), Coastal Tectonics. Geological Society, London, Special Publication 146, pp. 41–56.

Soter, S., 1999. Macroscopic seismic anomalies and submarine pockmarks in the Corinth–Patras rift, Greece. Tectonophysics 308, 275–290.

Soter, S., Katsonopoulou, D., 1998. The search for ancient Helike, 1988–1995: geological, sonar and bore hole studies. In: Katsonopoulou, D., Soter, S., Scilardi, D. (Eds.), Ancient Helike and Aigialeia, pp. 67–116. Proceedings of the Second International Conference, Aigion, December 1995.

Soter, S., Katsonopoulou, D., 1999. Occupation horizons found in the search for the ancient Greek city of Helike. Geoarchaeology 14, 531–563.

Stewart, I., 1996. Holocene uplift and paleoseismicity on the Eliki fault, western Gulf of Corinth, Greece. Annali di Geophysica 39, 575–588.

Stewart, I.S., Hancock, P.L, 1991. Scales of structural heterogeneity within neotectonic normal fault zones in the Aegean region. Journal of Structural Geology 13, 191–204.

Stewart, I., Vita-Finzi, C., 1996. Coastal uplift on active normal faults: the Eliki fault, Greece. Geophysical Research Letters 23, 1853–1856.

Stiros, S., Jones, E.R., 1996. Archaeoseismology. IGME–British School at Athens. Fitch Laboratory, occasional paper 7.